Experimental Study on Laser-Induced Spark Ignition of Some Flammable Premixtures

Tomohiko Imamura, Norimichi Morizumi, Yuki Miyazaki
Dept. of Mechanical and Electrical Engineering, Suwa University of Science,
5000-1 Toyohira, Chino-shi, Nagano, Japan

1 Introduction

The development of innovative combustion technologies that realize high efficiency and low emissions is expected to help achieve carbon neutrality. For example, superlean combustion effectively reduces combustion products which are the promoters of global warming, still difficult issues remain, such as how the ignitability and combustion instability can be improved. Laser-induced spark ignition (LSI) has attracted attention as a solution to these issues; therefore, many fundamental and practical studies have been conducted. For example, Lee et al. [1] conducted an LSI experiment using a ruby laser and obtained data on the minimum ignition energy (MIE). Phuoc [2] conducted experiments to determine the laser breakdown threshold under various ambient gas conditions. Endo et al. [3] investigated the ignition process of a propane–air mixture and compared it with the ignition process in which a capacitive spark is used. There have been many other studies on LSI [4–12]. As a result, many fundamental and useful findings on the ignition characteristics were obtained; however, many challenges remain. For example, it is necessary to clarify the influence of components on the laser-induced breakdown threshold of premixture, and to perform numerical simulations, to commercialize this technology. Because it has not been long since the investigation of LSI began, the ignition mechanism of LSI has not yet been established. Based on this background, an attempt was made to examine the dependence of the laser breakdown threshold and the MIE on the composition and variety of flammable mixtures to find the optimum ignition condition of LSI.

2 Experimental

Fig. 1 shows a schematic diagram of the LSI system. A second harmonic of a Q-switched Nd:YAG laser (Beamtech, Dawa-200) at 532 nm (maximum pulse energy: 100 mJ/pulse) was used. The pulse duration was 5.4 ns, measured using a photodetector, and the focusing diameter was 31.94 μm, measured using a beam profiler system. The pulse energy of the laser beam was controlled by adjusting a half-width waveplate and using a polarizing beam splitter. Subsequently, the pulse energy of the laser beam was divided into two beams, each with half the pulse energy. One was blocked by a pyroelectric energy sensor, and its pulse energy was measured. Hereinafter, this energy is denoted as E_i because it is equivalent to the incident energy of the combustion chamber. Another beam was passed through a focusing lens and then focused on the center of the combustion chamber. The focal length of the focusing

Correspondence to: imamura@rs.sus.ac.jp

lens was 100 mm. After the beam passed the focusing point, it was trapped by another pyroelectric energy sensor (Newport, 1919-R), and its pulse energy was measured. Hereinafter, this energy is denoted as E_t (the transmitted energy). A cylindrical combustion chamber (volume: 1.67 L, pressure resistance: 1 MPa) with four antireflection-coated quartz glass windows was used. A fan was installed at the bottom of the inside of the chamber. A pressure transmitter (KH-15, Nagano Keiki Co., Ltd.) and a K-type thermocouple were fixed at the top of the chamber. The ignition behavior was taken using the high-speed Schlieren imaging method (Photron, FASTCAM Nova S12). The commencement of laser oscillation, taking a high-speed movie, and recording charts of the evolutions of pressure and temperature were synchronized using a pulse generator.

In this study, the breakdown threshold and ignition energy were measured. First, the breakdown thresholds of hydrogen–air, methane–air, propane–air, and hydrogen–propane mixtures with various compositions were measured. Hydrogen–air, methane–air, and propane–air mixtures with various equivalence ratios were employed for ignition energy measurement. In this measurement, only one laser beam pulse oscillated to the mixture. In both experiments, the initial pressure and temperature were atmospheric pressure and room temperature (approximately 25 °C). The test mixture was stirred using a fan to ensure its homogeneity.

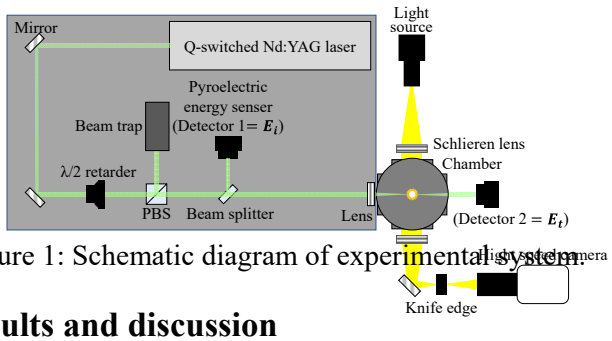

Figure 1: Schematic diagram of experimental system.

3 Experimental results and discussion

3.1 Laser breakdown threshold

Some of the breakdown thresholds have been reported previously. For example, the breakdown threshold reported by Kobayashi et al. [5] was approximately 14 mJ in the atmosphere, and the breakdown thresholds reported by Phuoc [2] were 17.79, 11.24, and 8.11 mJ for hydrogen, air, and methane, respectively. The breakdown threshold is determined as E_i, at which it starts to become greater than the E_t value reported in the literature [5]. In addition, it is defined as the laser energy at which the gas breaks down for more than 50% of the shots [2]. However, in this study, a laser-induced spark was observed, even at lower incident energy for each gas, as shown in Fig. 2. From the viewpoint of ensuring safe, a severer threshold of laser breakdown was determined as follows. First, a rough threshold in which 0-5 times breakdowns were observed in 75 pulses (repetition frequency:15 Hz, firing duration: 5 s) per one oscillation was obtained. Note that the breakdown was not always observed in this incident energy, rather than the cases that no breakdown was observed were greater. Although the Schlieren image determined the generation of plasma due to breakdown, we determined as breakdown even very small plasma shown in Fig. 2 from the viewpoint of contributing safe. Second, the incident energy in which the imperceptible breakdown was observed was obtained by carefully controlling incident energy around the above rough threshold. We obtained 20 numbers of the incident and the transparent energies in one test mixture, and the averaged value of the incident energy in these 20 numbers of data was determined as the breakdown threshold.

A laser-induced spark is generated either by the multiphoton ionization process or the electron cascade process [13,14]. The multiphoton ionization process influences the generation of sparks at short wavelengths (< 1 μm), which have a large photon energy [2]; thus, the larger the molecule, the more easily photon energy is absorbed, and the breakdown threshold becomes smaller. Furthermore, the ionization potentials of these gases influence the breakdown threshold. The ionization potentials of H_2, O_2, N_2, and CH_4 are 15.425, 12.07, 15.58, and 12.51 eV, respectively [2]. The ionization potential of air is estimated to be 14.84 eV, assuming that it can be calculated by the summation of the components of the ionization potential of air (79% N_2 and 21% O_2). The ionization potential of C_3H_8 is assumed to be as large as that of CH_4.

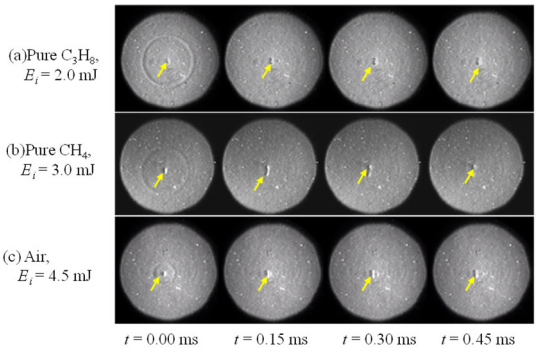

Figure 2: Generation of laser-induced spark in lower incident energy than the breakdown threshold in other previous studies. The yellow arrows show the spark generated by laser breakdown.

Table 1: Comparison of the breakdown threshold obtained in the present work with data reported by Phonc [2].

Gas	Breakdown threshold (laser intensity and pulse energy)			
	Present Work		Phonc [2]	
	(GW/cm^2)	(mJ)	(GW/cm^2)	(mJ)
H_2	78.8	3.42	5700	17.79
Air	39.8	1.73	3600	11.24
CH_4	29.3	1.28	2600	8.11
C_3H_8	16.3	0.71	–	–

Table 1 lists the breakdown thresholds of hydrogen, methane, propane, and air obtained in this study and by Phuoc [2]. In this experiment, the order of the value of the breakdown threshold was C_3H_8 < CH_4 < air < H_2, which coincides with the order of ionization potential values. Although the value of the breakdown threshold in this experiment was smaller than that reported by Phuoc [2], the dependence on the variety of fuels was similar in both datasets (CH_4 < air < H_2). The propane breakdown threshold was smaller than methane's because C_3H_8 could absorb photon energy easier than CH_4. This was because the molecular size of C_3H_8 is larger than that of CH_4. Fig. 3(a) shows the dependence of the breakdown threshold on the fuel concentration, and Fig. 3(b) shows the relationship between the absorption ratio ($A = (E_i - E_t)/E_t$) and fuel concentration. For the C_3H_8–H_2 mixture, the value of the horizontal axis in Fig. 3 coincides with the volumetric fuel concentration of C_3H_8 fuel, i.e., 100% of the horizontal axis corresponds to pure C_3H_8. For other mixtures, 0% and 100% on the horizontal axis correspond to pure air and pure fuel, respectively. For C_3H_8–air and CH_4–air mixtures, the breakdown thresholds decreased with increasing fuel concentration, whereas those of the H_2–air mixture increased. For the C_3H_8–H_2 mixture, the breakdown threshold decreased with increasing C_3H_8 concentration. The relationship between the change rate of the breakdown threshold which corresponds to the slope of Fig. 3(a) and fuel concentration was CH_4–air < C_3H_8–air < H_2–air < C_3H_8–H_2. The breakdown threshold of the mixture depends on the threshold of each pure gas of components and its composition. For C_3H_8–air, and C_3H_8–H_2, the difference of breakdown threshold of C_3H_8 and air (or C_3H_8 and H_2) is comparatively large, so the changing rate of breakdown threshold against fuel concentration is large. However, according to Fig. 3(b), the value relationship of the absorption ratios of pure gases was H_2 < air < CH_4 < C_3H_8, which is the opposite of the results of the breakdown thresholds. Fig. 4 shows the relationship between the

absorption energy and breakdown thresholds for various compositions of mixtures. The trend shown in Fig. 4 can be explained as follows. For the C_3H_8–air, CH_4–air, and C_3H_8–H_2 mixtures, the absorption ratio increases or is almost uniform with increasing fuel concentration, whereas the breakdown threshold becomes smaller, so the absorption energy is monotonously proportional to the breakdown threshold. However, for the H_2–air mixture, although the breakdown threshold increases with increasing H_2 concentration, the absorption ratio decreases; thus, the dependence of the absorption energy on the breakdown threshold is influenced depending on the above characteristics.

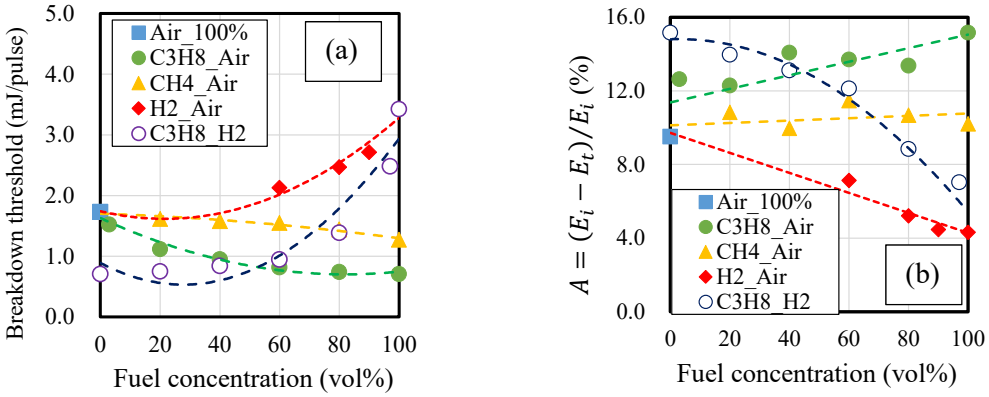

Figure 3: Dependences of breakdown threshold and absorption ratio on the fuel concentration.

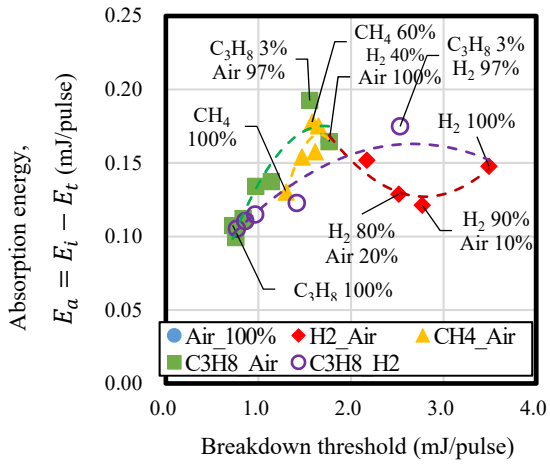

Figure 4: Relationship between the absorption energy and the breakdown threshold.

3.2 Visible behavior of evolution of flame kernel

Fig. 5 shows the flame kernels for H_2–air, CH_4–air, and C_3H_8–air, with various equivalence ratios, generated by the laser-induced spark at the minimum incident energy for ignition 1.0 ms or 2.0 ms after the laser oscillated. The laser direction was from right to left. A toroidal flame kernel that formed around the focal point of the laser beam can be observed in most of the photographs in Fig. 5, except for the cases of ϕ = 0.50–3.00 for H_2–air, in which the burning velocity is much larger. No image was obtained at ϕ = 1.75 for H_2–air because the flame kernel was already removed from the observation window owing to the larger burning velocity. In addition, the toroidal flame kernel becomes weak near the flammable limit, and a flame kernel protruding in the incident direction, the so-called "third lobe," which is peculiar to LSI [9,10], is shown by white arrows in Fig. 5. At ϕ = 5.85 for the H_2–air mixture, a flame kernel protruding in a "downstream direction," which was opposite to the third lobe, was observed, as shown by the yellow arrow in Fig. 5. It has been reported that this upstream flow can be observed as a "fourth lobe" when a continuous-pulse laser is used [8], but, to the authors' knowledge, it has not been reported in the case of a single-pulse laser.

3.3 Minimum ignition energy

Figs. 6(a)–(c) show the dependence of the MIE on the equivalence ratio for each fuel–air mixture. The energy plotted in Fig. 6 corresponds to $E_a = (E_i - E_t)$. The data obtained in other studies using LSI [1,12,17] and capacitive spark ignition [15,16] are plotted together for comparison. For the C_3H_8–air mixture, the present data almost coincided with the data obtained by Lee et al. [1] (532 nm, focal length: 50 mm, pulse duration: <10 ns) near the stoichiometric composition, but they were larger near the flammable limit. This might have been caused by the difference in the focal length. The present data and the data of Lee et al. were larger than those of Lewis and Elbe, in which a capacitive spark was used. For the CH_4–air mixture, the present data were larger than the data obtained by Saito et al. [12] (focal length: 50 mm, pulse duration: 5 ns), who used a laser-induced spark, and those of Lewis and Elbe [16]. The MIE of the present data was taken as a local minimum near ϕ = 0.9, which was similar to that obtained by a capacitive spark [16]. For the H_2–air mixture, the present data almost coincided with the data obtained by Rooney [17], who used a laser-induced spark, but were slightly larger than the data of Ono et al. [15], who used a capacitive spark. In particular, the difference between the present data and the data obtained using a capacitive spark [15] gradually increases on the fuel-rich side in each mixture.

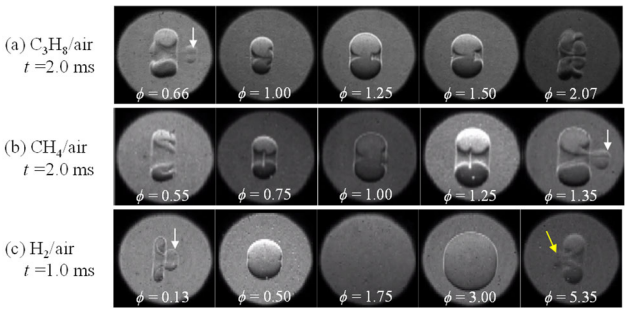

Figure 5: Visible behavior of evolution of flame kernel generated by laser-induced spark with minimum ignition energy.

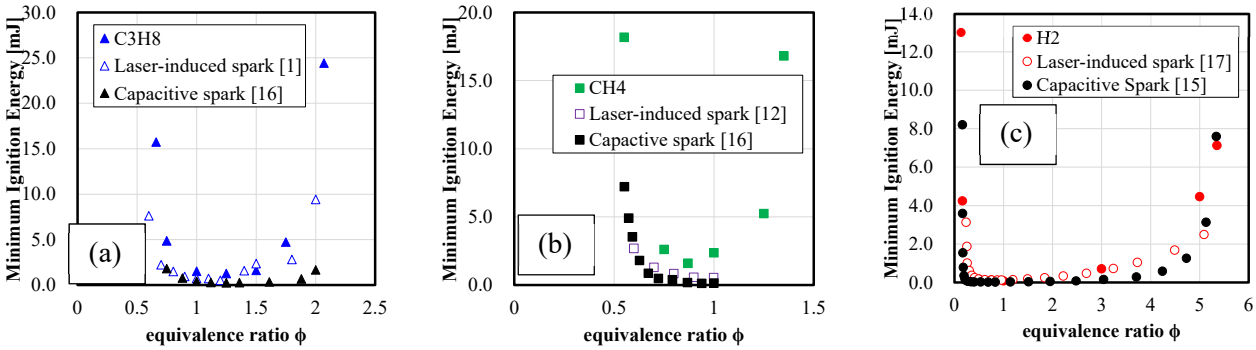

Figure 6: Dependencies of the minimum ignition energy and equivalence ratio in various mixtures: (a) C_3H_8–air, (b) CH_4–air, and (c) H_2–air.

4 Conclusions

(1) The breakdown thresholds for hydrogen–air, methane–air, propane–air, and hydrogen–propane mixtures with various compositions were measured. The breakdown threshold of the pure gases was in the ascending order of C_3H_8, CH_4, air, and H_2, which were determined based on the molecular size and ionization potential of the molecules. The breakdown thresholds of these mixtures were influenced by composition and the difference of breakdown thresholds of pure components.

(2) A kernel flow in the downstream direction was observed at ϕ = 5.85 for the H_2–air mixture, which is opposite to the so-called "third lobe." Although it has been observed for a multipulse incident laser beam, it is believed that for the first time, it is observed for a single-pulse laser.

Acknowledgments

Part of this study was conducted as part of the project “Development of Technology and Assessment Techniques for Next-Generation Refrigerants with a Low GWP Value” conducted by NEDO.

References

[1] Lee TW, Jain V, Kozola S (2001). Measurements of minimum ignition energy by using laser sparks for hydrocarbon fuels in air: Propane, dodecane, and jet-A fuel. Comb. Fla. 125(4): 1320–8.

[2] Phonc TX (2000). Laser spark ignition: Experimental determination of laser-induced breakdown thresholds of combustion gases. Opt. Commun. 175: 419–23.

[3] Endo T, Takenaka Y, Sako Y, Johzaki T, Namba S, Shimokuri D (2017). An experimental study on the ignition ability of a laser-induced gaseous breakdown. Comb. Fla. 178:1–6.

[4] Morkani N, Gillard P (2020). Laser induced breakdown in gas mixtures: Experimental and statistical investigation on n-decane ignition: Pressure, mixture composition and equivalence ratio effects. J. Haz. Mat. 388: 119266.

[5] Kobayashi Y, Tsujino T, Nakaya S, Tsue M, Takahashi S (2019). Laser-induced spark ignition of DME-air mixtures in microgravity: Comparison of ignition characteristics between normal gravity and microgravity. Fuel 236: 1391–9.

[6] Mulla IA, Chakravarthy SR, Swaminathan N, Balachandran R (2016). Evolution of flame-kernel in laser-induced spark ignited mixtures: A parametric study. Comb. Fla. 164: 303–18.

[7] Shukla A, Vaghasia J, Mistry M (2022). Effect of laser ignition on combustion and performance of internal combustion engine: A review. Ene. Conv. Man.: X 13: 100166.

[8] Singh AP, Padhi UP, Joarder R (2022). Insight into the evolution of laser-induced plasma during successive deposition of laser energy. J. Appl. Phys.131: 073301.

[9] Beduneau JL, Kim B, Zimmer L, Ikeda Y (2003). Measurements of minimum ignition energy in premixed laminar methane/air flow by using laser induced spark, Comb. Fla. 132: 653–65.

[10] Bradley D, Sheppard CGW, Suardjaja IM, Wooley R (2004). Fundamentals of high-energy spark ignition with lasers. Comb. Fla. 138(1-4): 55–77.

[11] Fernandez-Tarrazo E, Gomez-Miguel R, Sanchez-Sanz M (2023). Minimum ignition energy of hydrogen-ammonia blends in air. Fuel 337:127128.

[12] Saito T, Furutani H (2009). Dynamics of ignition and combustion by laser induced plasma. J. Comb. Soc. Jpn., 51(158): 281–7, in Japanese.

[13] Dewhurst R (1978). Comparative data on molecular gas breakdown thresholds in high-laser radiation fields. J. Phys. D: Appl. Phys. 11: 191–5.

[14] Peet VE, Tsubin RV (1997). Multiphoton ionization and optical breakdown of xenon in annular laser beams. Opt. Commu. 134: 66–8.

[15] Ono R, Nifuku M, Fujiwara S, Horiguchi S, Oda T (2007). Minimum ignition energy of hydrogen-air mixture: Effects of humidity and spark duration. J. Electrostat. 65(2):87–93.

[16] Lewis B, von Elbe G (1987). Combustion, Flames and Explosions of Gases. 3rd Ed. Academic Press (ISBN 9780323138024).

[17] Rooney PD (1994). Laser versus conventional ignition of flames. Opt. Eng. 33(2): 510–21.